

In-situ damage self-monitoring of fiber-reinforced composite by integrating self-powered ZnO nanowires decorated carbon fabric

Xiaoming Chen^a, Siyi Cheng^a, Kaiqiang Wen^a, Chunjiang Wang^a, Jie Zhang^{b,*}, Han Zhang^a, Hechuan Ma^a, Lei Wu^c, Tianliang Li^d, Baotong Li^{e,**}, Jinyou Shao^a

^a Micro- and Nanotechnology Research Center, State Key Laboratory for Manufacturing Systems Engineering, Xi'an Jiaotong University, Xi'an, Shaanxi, 710049, China

^b Electronic Materials Research Laboratory, Key Laboratory of the Ministry of Education & International Center for Dielectric Research, School of Electronic Science and Engineering, Xi'an Jiaotong University, Xi'an, Shaanxi, 710049, China

^c School of Petroleum Engineering, China University of Petroleum (East China), Qingdao, 266580, China

^d School of Mechanical and Electronic Engineering, Wuhan University of Technology, Wuhan, China

^e Key Laboratory of Education Ministry for Modern Design & Rotor-Bearing System, Xi'an Jiaotong University, Xi'an, Shaanxi, 710049, China

ARTICLE INFO

Keywords:

ZnO nanowire
Piezoelectric effect
Self-powered sensing
Fiber-reinforced composite
In-situ damage detection

ABSTRACT

The tradeoff between damage self-sensing abilities and mechanical properties of composites is still a challenge for incorporating functional materials as potential sensing components. In this work, multifunctional carbon fabric coated with piezoelectric zinc oxide nanowires (ZnO NWs) was integrated into a carbon fiber reinforced composite as simultaneously a self-powered damage sensing component and mechanical reinforcement. The embedded ZnO NWs endowed the composite with *in-situ* self-sensing of damage. The sensing characteristics corresponding to the composite damage were validated by a well-established acoustic emission method. The results showed comparable performances to those obtained by common damage detection techniques. Additionally, the introduction of ZnO NWs had a positive impact on the mechanical properties of the host composite, increasing tensile and flexural strengths by 7.4% and 4.8%, respectively. These values were significantly higher than those of the interleaved strong piezoelectric PVDF thin films, leading to severe degradation in both tensile strength (-28.6%) and flexural strength (-82.4%). The enhanced mechanical properties may be ascribed to the interfacial mechanical interlocking and the increased bond area induced by the penetration of stiff ZnO NWs into the resin matrix. Overall, the excellent online and *in-situ* damage self-monitoring abilities with inherent structural benefits make ZnO NWs-based sensing scheme promising for broad applications in the field of structural health monitoring.

1. Introduction

Fiber-reinforced polymer matrix composites with high strength-to-weight ratio and excellent mechanical properties play a crucial role in many engineering fields, including automobile, aircraft, and aerospace [1]. However, the one-by-one stacking nature of composite laminates might induce various types of failure modes, such as fiber breaking, interface debonding, and delamination, thereby limiting their applications. To preserve high performance and structural safety, the damages need to be detected in the early stages. Thus, the composites need to be periodically inspected for detecting the existence of damage. Over the past several decades, numerous mature and reliable techniques have

been developed to fulfill damage and failure detection [2–5], including infrared thermal imaging, ultrasonic testing, acoustic emission testing, and X-ray scanning. However, these methods are mainly limited by off-line and non-*in-situ* damage detection features, leading to increased maintenance costs and decreased reliability. To overcome these deficiencies, substantial research efforts have been devoted to studying structural health monitoring (SHM) to constantly inspect the composite conditions throughout the entire service life and identify damage in real-time.

Two kinds of real-time damage monitoring techniques are currently used for fiber-reinforced composites: i) external sensors-based and ii) internal sensors-based health detection. Acoustic emission testing (AET)

* Corresponding author.

** Corresponding author.

E-mail addresses: jzhang12@xjtu.edu.cn (J. Zhang), baotong.me@xjtu.edu.cn (B. Li).

has been well established as one of the most used health monitoring via using externally bonded sensors. This technique not only provides real-time sensitive information regarding the state of structural health but also demonstrates nonintrusive attributes in terms of the mechanical properties of host composite structures. However, despite the excellent ability of externally bonded sensors-based AET in detecting damage, they still suffer from frequent exposure to complex and pernicious environmental factors that result in decreased long-term sensing effectiveness and accuracy or even non-functionality. In addition, externally bonded sensors-based AET greatly relies on the experience of manipulating personnel and sometimes is not convenient for practical applications.

In view of this, to fully overcome the limitations induced by external bonding, increasing efforts have been devoted to using internal embedded sensors for *in-situ* damage detection of fiber-reinforced composites with more reliable signals and longer service life. Optical fiber, such as fiber Bragg grating (FBG) has widely been studied as the fully embedded sensor in a fiber-reinforced composite of in-service composites' damage sensing [6–12]. Such alternative embedded fiber demonstrated the effectiveness of continuously monitoring the strain and damage as external bonded sensors. However, the implantation of the optical fiber may destroy the integrity of composite materials due to the brittleness and rigidity of optical fiber, negatively affecting the mechanical properties. In addition, features like the discrete nature of embedded fiber sensor, specific fiber orientation, arrangement and positioning of fibers are required for large-area and accurate damage sensing. Among internal sensor-based *in-situ* monitoring techniques, electrical signals based on either resistance or voltage-based measurements relying on piezoresistive or piezoelectric materials have attracted increasing attention in sensing to demonstrate the ability of damage detection. Piezoresistivity-based monitoring techniques mainly rely on either the inherent sensing function of composites or the integration of sensing elements into composites. The inherent sensing properties are introduced into composite by adding conductive fillers [13–16] (e.g., graphene or carbon nanotube) into electrically insulating matrix or conductive fiber reinforcements (e.g., carbon fiber) [17,18]. The highly conductive fillers or fibers form electrical networks within the composites. As a result, the subjection of the composites to external loading leads to damage occurrence, which induces conductive pathways breaking in the electrical network, resulting in increased inherent resistance in the test specimen [19–21]. In comparison to inherent sensing properties, alternative embedded resistance components have intensively been studied in recent years. For example, several research groups show the excellent abilities of damage monitoring and failure warning by interleaving carbon nanotube/graphene-based buckypaper and grid [22,23]. However, the inclusion of foreign sensing elements may degrade the mechanical properties of composites and potentially increase the risk of damage and failure. Additionally, piezoresistivity-based monitoring measurements require additional power sources or excitation voltages to generate output signals in response to damages. Thus, long-term reliance on necessitating power remains a technical challenge for continuous monitoring structural state.

By comparison, piezoelectricity-based measurements work in self-powered mode, allowing continuous monitoring of the functional state of composites by converting damage-induced release of mechanical energy to an electrical signal via the direct piezoelectric effect. As a result, piezoelectricity-based sensing measurements do not require an external excitation source [24–30]. Besides, the better piezoelectric performance of piezoelectricity-based sensors induces a higher signal-to-noise ratio coupled with good sensitivity and fast response time. However, only a handful of reports have so far investigated the damage monitoring of fiber-reinforced composites using piezoelectric materials [31–35]. It is noted that polyvinylidene fluoride (PVDF) is a promising piezoelectric material for damage monitoring owing to its good flexibility and high electromechanical coupling coefficient.

PVDF-based sensors in the forms of fiber, yarns and fabric have received considerable interests and demonstrated the extraordinary ability of *in-situ* strain and damage degree monitoring as aforementioned piezoresistivity-based sensors with the additional external power requirements [33–35]. In spite of these valuable advances, two limitations and challenges remain yet to be solved. First, implantation of PVDF materials into composites provides no inherent structural benefit or even degrades the mechanical properties. Second, the poor thermal stability of piezoelectrical properties gives rise to partial or full depolarization, thereby limiting the practical applications in fiber-reinforced composites.

Herein, piezoelectric ZnO NWs decorated fabric was fabricated as an *in-situ* sensor for tracking the damage of the host composite, as well as a reinforcing layer for improving the composite's mechanical properties. As schematically shown in Fig. 1a, ZnO NWs were first grown onto woven carbon fabric by a two-step growth method followed by integration into the carbon fiber reinforced composite. The resulting hybrid composite laminate was beneficial to self-monitoring the damage without requiring external input power. The mechanical-electrical behaviors of the composites and the corresponding damage monitoring sensitivities were investigated by uniaxial tensile and three-point bending tests. The results revealed an obvious enhancement in mechanical properties of composites and additional ability of *in-situ* damage self-monitoring, confirmed by the commercially available acoustic emission (AE) technique. Overall, by considering the positive attributes in mechanical properties and the ability of damage self-monitoring, the ZnO nanowires decorated carbon fabric exhibits great perspectives in the field of structural health monitoring for carbon fiber reinforced composite.

2. Experimental

2.1. Materials

PAN-based plain-woven carbon fabrics based on T300 type (Toray Co.) were used in this study. The desized fiber and fabrics were obtained by soaking pristine fibers and fabrics in acetone for 24 h, followed by rinsing with methanol and deionized (DI) water several times and drying in an oven for 1 h. To enhance the binding strength between zinc oxide nanowire and carbon fiber surface, polydopamine (PDA) treatment solution was formulated with dopamine, hydrochloric acid, and Trihydroxymethylaminomethane (Tirs-buffer). For the synthesis of zinc oxide nanowires on carbon fabrics, ZnO seed solution and growth solution were first prepared separately. The ZnO seed solution was obtained by dissolving zinc acetate dehydrate (0.45 g) and sodium hydroxide (0.14 g) in 2.5 L of ethanol at 60 °C under vigorous stirring. The growth solution was obtained by mixing zinc nitrate hexahydrate (0.05 M) and hexamethylenetetramine (HMTA, 0.05 M) aqueous solution. Epoxy resin (E51) was used as a matrix. Dimethyl dicarbonate (DMDC), was employed as the curing agent. Conductive silver paste was utilized as an electrode. To prepare piezoelectric films, Poly(vinylidene fluoride-co-trifluoroethylene) (P(VDF-TrFE), type FC30, Arkema, France) was dissolved in Dimethylformamide (DMF).

2.2. Growth of ZnO nanowires on carbon fabric

To obtain strong interfacial binding strength of ZnO nanowires (NWs) with carbon fiber, PDA layer was used as an interfacial promoter. PDA coating was deposited on carbon fiber by first cutting desized plain-woven carbon fabrics into sizes of 10 × 10 cm² followed by immersing in a mixed solution containing Tris-buffer with a pH of 8.5 for 24 h at room temperature. Next, the fabrics were rinsed with DI water and dried at 100 °C for 30 min. The growth of ZnO NWs on carbon fabric consisted of two hydrothermal synthetical steps. The first involved ZnO seed coating and the second had to do with ZnO NWs growth. The first step allowed the formation of a ZnO crystal seed layer on the carbon fabric surface. In

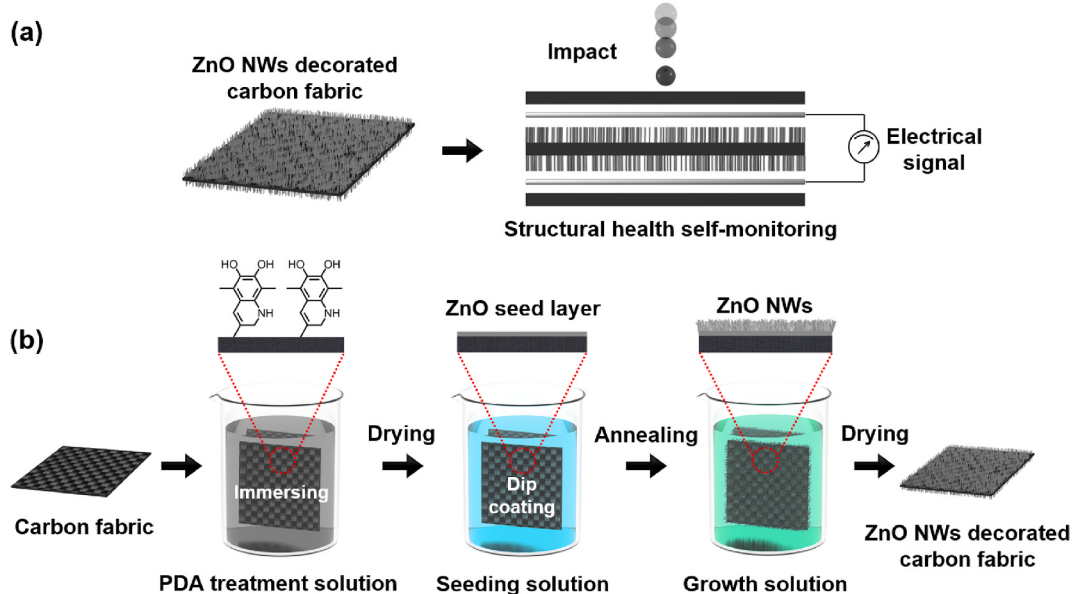


Fig. 1. (a) Schematic representation of ZnO nanowires (NWs) decorated carbon fabric-based *in-situ* structural health self-monitoring method. (b) Schematic representation of the fabrication procedure of ZnO NWs on carbon fabric.

this process, carbon fabrics with PDA layer were dipped in the seed solution and annealed at 150 °C for 10 min. To obtain a uniform and ultrathin ZnO seed layer on carbon fabric, the dip-coating was repeated thrice. The fabric with ZnO seed layer was then submerged in the ZnO growth solution followed by heating in a convection oven for 4 h at 90 °C. After rinsing with DI water and drying at 100 °C for 30 min, a ZnO NWs layer decorated carbon fabric was finally obtained.

2.3. Preparation of ZnO-based and P(VDF-TrFE)-based composite laminates

The carbon fiber-reinforced composite interleaved with ZnO NWs decorated carbon fabric (ZnO-based composite) consisted of two plies of plain-woven carbon fiber fabrics and one ZnO NWs decorated carbon fabric (ZnO-decorated CFA) sensing layer through hot-press process. To obtain ZnO-decorated CFA sensing layer, the epoxy resin (E51) with the curing agent (DMDC) at the ratio of 3:1 was poured on ZnO-decorated CFA. Next, the fabric/epoxy was compressed and partially cured by hot pressing at a pressure of 100 kPa and a temperature of 70 °C for 3 h. A thin conductive silver paste layer acting as an electrode was finally coated on each side of partially cured ZnO-decorated CFA/epoxy composite layer. The as-obtained composite layer working as a sensing layer was inserted into the composite laminate as the middle ply and outer two plain-woven carbon fabrics as the top and bottom plies of the final composite. The obtained composite laminates were cured with epoxy resin at 90 °C for 3 h under a pressure of 100 kPa. For comparison, composite laminate without a ZnO-decorated CFA sensing layer (baseline composite) and composite laminate containing silver electrodes (Ag-interleaved composite) were prepared by following the same methodology. As a reference, a composite laminate with two P(VDF-TrFE) interleave (P(VDF-TrFE)-based composite) was also prepared. To this end, 0.5 g P(VDF-TrFE) powder was dissolved in 10 mL DMF and stirred at 60 °C for 12 h to fully dissolve P(VDF-TrFE). The resulting solution was spin-coated on a silicon wafer at a speed of 300 r/min for 60 s and then dried on the heating plate for 2 h to fully evaporate DMF solvent, yielding a film thickness of about 30 μm. Afterward, the two 30 μm thick P(VDF-TrFE) films were sandwiched between layers of plain-woven carbon fabric as the second and fourth plies in the composite laminate. The outer layers of carbon fabric were used as electrodes. The laminates were fully infiltrated with resin followed by curing at 90 °C

and 100 kPa for 3 h to yield P(VDF-TrFE)-based composite laminate. Finally, the prepared laminate was polarized at 90 °C under an electric field of 20 V/μm for 6 h to make P(VDF-TrFE) with better piezoelectric properties.

2.4. Characterization and mechanical testing

The surface morphologies, fractured cross-sections, and elemental compositions of the as-obtained samples were investigated by scanning electron microscopy (SEM; SU8010, Hitachi) equipped with an energy-dispersive X-ray spectroscopy (EDS) detector. The crystal structures of the samples were analyzed by X-ray diffraction (XRD; D8 advance A25, HK) in the 2θ range of 10°–70°. Single fiber tensile testing was conducted on a precision tensile microstage (Linkam MFS 350, UK). At least 30 specimens were tested for each fiber type, and the results were analyzed by Weibull's statistics. The interfacial shear strength (IFSS) of each sample was evaluated by microdroplet debonding testing using interfacial evaluation equipment (HM410, Japan). The average IFSS values were calculated by assuming uniform stress on the entire interface [36],

$$\text{IFSS} = F_{\max}/(\pi d l) \quad (1)$$

where F_{\max} represents the maximum debonding load, d is the relevant fiber diameter, and l is the embedded length.

Piezoelectric properties of ZnO-based and P(VDF-TrFE)-based composite laminates were assessed on a homemade testing system. The piezoelectric voltages were measured with a four-channel oscilloscope (Tektronix DPO 3034). Tensile and bending tests were performed on a universal testing machine (INSTRON, Microtester 5848). The loading speeds of the tensile and bending tests were set to 1 mm/min and 3 mm/min, respectively. To demonstrate the damage monitoring reliability of the composite with ZnO decorated carbon fabric during mechanical testing, an acoustic emission (AE) equipment (MB2-V2, ASIP-2/S, Vallen System GmbH) was used to monitor the damage with the AE probe (with a frequency of 100 kHz) fixed to the surface of the laminates.

3. Results and discussion

A schematic representation of the preparation process of ZnO NWs on plain-woven carbon fabric is provided in Fig. 1b. Briefly, a plain-

woven carbon fabric was first immersed in the PDA treatment solution for 24 h. During this period, dopamine was self-polymerized on the carbon fiber (CF) surface to form a thin layer of PDA. A ZnO seed layer was then deposited by immersing the PDA-modified carbon fabric in the seed solution followed by thermal annealing at 150 °C for 10 min. This step was repeated three times to yield a uniform ZnO seed crystal layer covering the carbon fabric. The PDA layer promoted the formation of a ZnO seed layer and enhanced the interfacial binding strength of individual carbon fiber with ZnO NWs [37,38]. The resulting carbon fabric was finally placed in a sealed glass container with a growth solution at 90 °C for several hours to react. It is noted that the duration of hydrothermal growth time greatly influenced the thickness of ZnO nanowire layer. After washing with deionized water and drying at 100 °C for 30 min, ZnO NWs decorated carbon fabric was successfully obtained.

The SEM morphology of ZnO NWs grown on the carbon fabric surface for 4 h is depicted in Fig. 2a. A relatively uniform layer of ZnO NWs conformally covering the entire surface of carbon fabric was noticed. To clearly observe the detailed morphology of ZnO NWs on carbon fiber surface, a single fiber was extracted and examined in the SEM. As shown in Fig. 2b–c, the carbon fiber was completely covered by a thin ZnO NWs layer with a randomly orientated needle-like structure. Compared to the pristine T300 carbon fiber with a diameter of 7 μm (Fig. S1a), the thickness of ZnO NWs layer was estimated to be 1 μm. The ZnO seed layer looked very thin with limited effect on the surface morphology of carbon fiber (Fig. S1b). ZnO NWs synthesized on carbon fiber surface at the different growth times of 2 and 6 h are gathered in Fig. S1c–d. The corresponding diameters of fiber were measured as $8.75 \pm 0.32 \mu\text{m}$ and $9.69 \pm 0.28 \mu\text{m}$, respectively. In EDS element mapping of nanowires on individual carbon fiber (Fig. 2d–f), Zn and O elements looked uniformly distributed in the fiber area. Since fiber was fully covered by ZnO NWs coating, nearly no C element was detected in the corresponding fiber region. Moreover, the crystalline phases of carbon fibers and obtained ZnO NWs were also confirmed by XRD. In Fig. S2, a diffraction broad peak around 26° was noticed in all three curves, assigned to graphite (002) planes of carbon fibers. Besides, no additional peaks were noticed in the spectrum of PDA-modified carbon fiber, probably due to the limited amount of coating. Meanwhile, numerous characteristic peaks appeared in the carbon fiber coated with ZnO NWs. The observed peaks could be indexed to the hexagonal wurtzite phase of ZnO, where the three typical peaks at 31.8°, 34.5°, and 36.3° corresponded to the (100),

(002), and (101) planes, respectively [39].

The practical promoting effects of PDA thin layer and the influence of ZnO NWs layer on the mechanical properties of composite were investigated by testing the interfacial properties of PDA-modified CF-epoxy (EP) and ZnO NWs coated CF-EP composites via microdroplet debonding testing (Fig. S3a). Fig. 3a and S3b show the dependence of IFSS on the different ZnO NWs thickness obtained by varying growth times raining from 0 to 6 h and the presence of the PDA layer. As shown in Fig. S3b, the ultrathin ZnO seed layer showed nearly no effect on the interfacial properties, and IFSS value remained at around 60.15 MPa. This may be ascribed to the seed layer, which was too thin to alter the surface morphology of carbon fiber. Additionally, by increasing the hydrothermal growth time, the IFSS of ZnO-2h- (growth time of 2 h), ZnO-4h- (growth time of 4 h) and ZnO-6h- (growth time of 6 h) based interface remarkably decreased to 41.52, 59.62 and 40.27 MPa, respectively. The noticeable degradation in interfacial properties can be assigned to two factors. First, the weak interaction between ZnO layer and carbon fiber induced interfacial delamination [40,41]. Second, the poor wettability of epoxy resin on dense and long ZnO nanowires might result in incomplete infiltration of resin into nanowires, as well as relatively weak mechanical interlocking with resin matrix [42]. The surface morphology of ZnO-2h-coated carbon fiber debonding from the resin matrix is illustrated in Fig. S3c. The debonded fiber surface looked relatively clean without obvious resin and ZnO NWs, indicating weak interactions between the ZnO NWs layer and fiber. To enhance the interfacial binding strength of ZnO layer with carbon fiber by converting weak van der Waals interaction to chemical bonding, PDA thin layer was deposited on the CF surface for consequently promoting the growth of ZnO NWs [43]. As shown in Fig. S3b, the PDA treatment positively affected the interfacial strength of the pristine and ZnO seed layer coated CF with the resin. Additionally, the PDA coating noticeably improved the IFSS of ZnO NWs coated CF with the resin. Compared to the fiber without PDA layer, the IFSS values of ZnO/PDA-2h-, ZnO/PDA-4h- and ZnO/PDA-6h-based composite interfaces increased by 9.0%, 21.3%, and 11.5% respectively. Especially, the IFSS of ZnO/PDA-4h coated carbon fiber reached 72.33 MPa, a value 20.2% higher than that of pristine carbon fiber (Fig. 3a). The debonded surface of ZnO/PDA-4h coated CF-EP interface is depicted in Fig. 3b. The resin completely infiltrated the nanowires, and large amounts of epoxy and ZnO nanowire fragments were present on the fiber, suggesting a strong mechanical interlocking

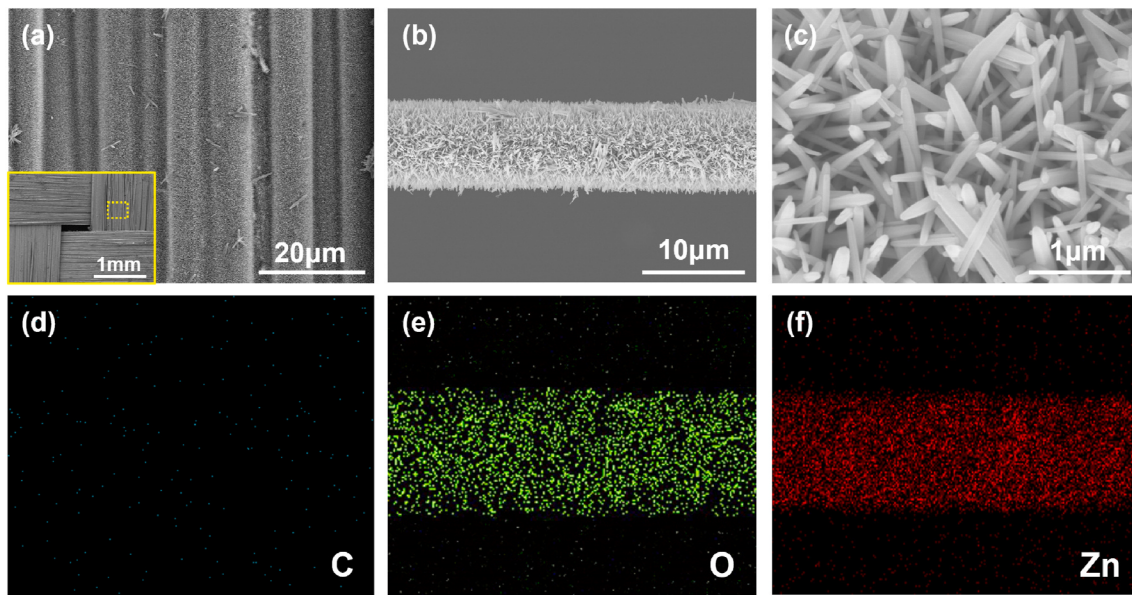


Fig. 2. SEM images of (a) carbon fabric with ZnO NWs, (b) single carbon fiber with ZnO NWs, and (c) magnified ZnO NWs. The hydrothermal growing time of ZnO is set to 4 h. (d–f) EDS element mapping images of single carbon fiber with ZnO NWs, indicating a homogeneous distribution of elements (C, O, and Zn).

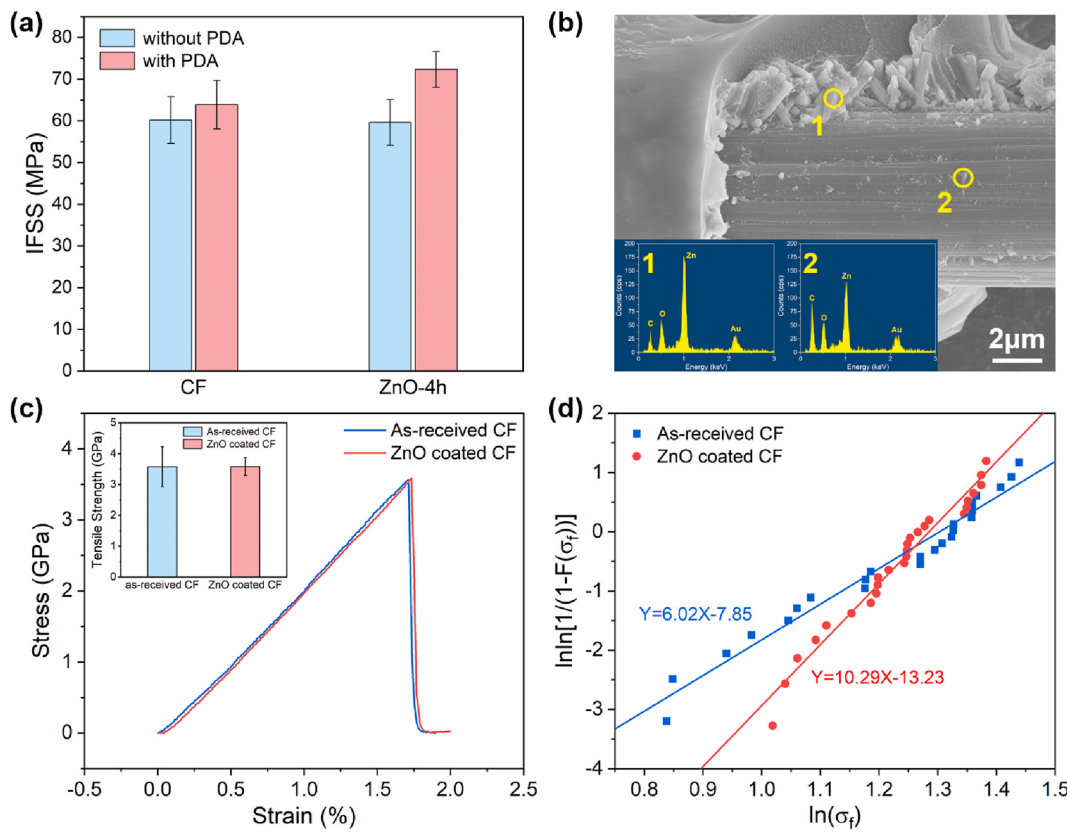


Fig. 3. (a) Effects of PDA treatment and ZnO NWs on IFSS of CF-EP composites. (b) The debonded surface of ZnO/PDA-4h coated CF-EP interface. The insets represent EDS elements characterization. (c) Tensile stress-strain curves of pristine carbon fiber and ZnO NWs coated-CF. The inset shows the tensile strength of carbon fiber with and without ZnO NWs coating. (d) Weibull distribution plots of pristine and ZnO/PDA-4h coated-CF.

between fiber and resin matrix.

The effects of the hydrothermal growth process on the mechanical properties of carbon fiber monofilaments were investigated by single fiber tensile testing. To obtain reliable results and better assess the variation of tensile strength, more than 30 test specimens were tested for each type of carbon fiber. Typical tensile stress-strain curves and corresponding Weibull distribution plots of pristine and ZnO/PDA-4h coated carbon fiber are gathered in Fig. 3c-d. Obviously, two stress-strain curves overlapped with the nearly same slope and ultimate strain, indicating no discernible changes in the mechanical properties of carbon fiber during the growth of ZnO nanowires. The single fiber tensile strengths of the as-received CF and ZnO/PDA-4h coated CF were calculated as 3.57 ± 0.65 GPa and 3.58 ± 0.29 GPa, respectively. These values were consistent with previously reported T300 tensile strength [44,45]. Besides, Weibull distribution plots were presented for evaluating scatter degree of the fiber tensile strength, which can indicate the number of flaws in the CF structure. The values of the Weibull modulus represented by the slope of the fitted straight lines increased from 6.02 for the pristine carbon fiber to 10.29 for ZnO/PDA-4h coated CF with a 70.9% increment. Thus, the introduction of the ZnO NWs layer improved the reliability of a single fiber to yield better mechanical properties by bridging the flaws/cracks on the surface [46].

To demonstrate the sensing ability of ZnO-decorated CFA sensing layer in the composite laminae, as well as investigate its effect on the mechanical properties, the composites interleaved with ZnO-decorated CFA (ZnO-based composite) were prepared. The preparation process was carried out according to the manufacturing methodology described in Section 2.3. To better analyze the benefits of using ZnO-decorated CFA as an embedded sensing material, the composite laminates with interleaved P(VDF-TrFE) film (P(VDF-TrFE)-based composite), which is widely adopted as functional materials due to its high piezoelectric

coupling, were also prepared for providing a reference for comparison during all testing. The explosion diagrams of ZnO-based composite and P(VDF-TrFE)-based composite are provided in Fig. 4a and S4a. Both composite laminates consisted of three carbon fabrics and two foreign interleaves. As shown in Fig. S4b, the cross-section images of P(VDF-TrFE) interleaf in composite displayed two layers of P(VDF-TrFE) sandwiched in the laminate with a thickness of around 30 μm. The outer layers of carbon fabrics worked as conductive electrodes in P(VDF-TrFE)-based composite laminate instead of interleaved thin silver paste in ZnO-based composites (Fig. 4b-c). A schematic representation of the experimental test setup employed for determining the sensing characteristics of composite laminates is displayed in Fig. 4d. According to the sensing principle of ZnO NWs and P(VDF-TrFE) piezoelectric materials, a sudden voltage emission across the samples was generated when the sensing materials were subjected to external pressure, strain, and even damage. In this experiment, periodically vertical mechanical pressure at a 1 Hz frequency was applied to the functional composite laminate using an electromechanical vibrator. The absolute output voltages of the laminate under the cyclic pressing and releasing process with five compressive loads of 9.2, 30.2, 47.8, 72.0, and 89.0 kPa are summarized in Fig. 4e. Obviously, the generated piezoelectric voltages increased linearly with the applied force, demonstrating a sensitivity (defined as the ratio of output voltage to applied mechanical pressure) of 2.83 mV/kPa.

Furthermore, the stability of the piezoelectric signal was verified by subjecting the laminate samples to 5000 cycles under a 1 Hz cyclic pressing and releasing forces with a pressure of 60 kPa (Fig. 4f). The output voltage remained stable as a function of time. The inset enlarged views demonstrated the presence of positive and negative peaks corresponding to compression and release processes of the applied force. The great stability confirmed the ability of the samples in strain and damage

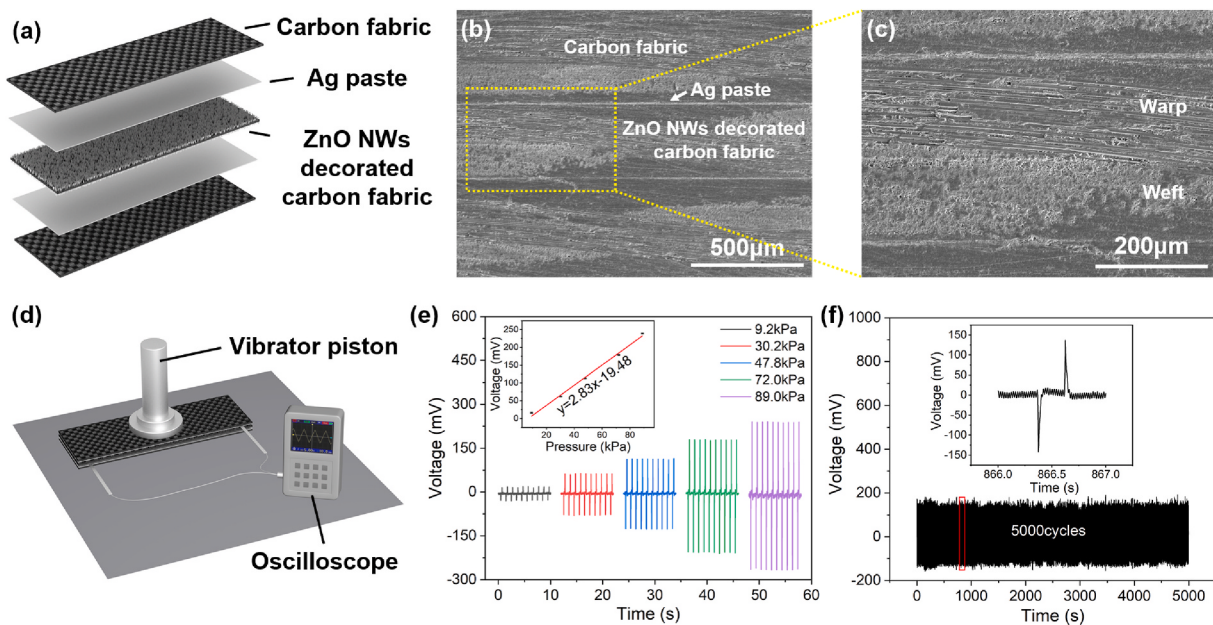


Fig. 4. (a) Explosion diagram of ZnO-based composite laminates. Cross-sectional image (b) and zoomed view (c) of composite laminate. (d) Schematic of mechanical-electrical response measurements. (e) Dependence of output voltages on different applied forces. (f) Stability tests under a 1 Hz pressing/releasing loading at a pressure of 60 kPa.

sensing. By comparison, the piezoelectric performance of P(VDF-TrFE)-based composite laminate specimens (Fig. S4c) revealed output voltage linearly and rapidly rising from 150 to 830 mV at pressures from 6.3 to 27.1 kPa, indicating a high sensitivity of 32.79 mV/kPa. The piezoelectric properties of P(VDF-TrFE)-based composite were nearly 11.5-fold higher than those of ZnO-based composite. This can be ascribed to the strong piezoelectric characteristics and high amounts of P(VDF-TrFE) layer [47].

To determine the ability of *in-situ* damage self-monitoring (e.g., resin matrix cracking, interfacial debonding, and fiber failure) of the composite by using ZnO NWs functional materials, the tensile and three-point bending tests for ZnO-based composite were conducted, along with output voltage measurements. The high rise in output voltage in all tests is corresponding to the occurrence of damage. Additionally, a commercially available acoustic emission (AE) detector was attached to the specimens for independently monitoring damage signals during all tests. Composite damage in the form of debonding, delamination, fiber failure, crack initiation or propagation can result in a sudden release of energy leading to propagating elastic stress waves, which can be detected by dedicated AE probes attached to the surface of the composite. The detectable AE signals are responsible for released energy resulting from composite damage [21,32]. AE monitoring was well established for identifying initiation and propagation of cracks in composites by detecting propagating damage induced-sudden release of energy, which is used to justify the reliability of ZnO NWs in damage self-sensing. A schematical tensile and bending test setup assembled by including AE sensor is shown in Fig. 5a–b. The measured stress, voltage, and AE energy values as a function of the strain for composite laminates without ZnO NWs under tensile and bending tests are depicted in Fig. 5c–d. The readings of AE energy clearly showed the progression of mechanical loading induced the point of damage. However, the output voltages in the majority of test durations were maintained at the bottom background noise level due to the lack of piezoelectric component. Few weak voltage readings were recorded in both the tensile and bending tests. Due to the absence of ZnO NWs, we reasonably speculated that the weak voltage signals may be induced by triboelectric effect, which originated from contact electrification between the two objects and produces non-negligible interfacial electron transfer in the stages of contacting and separating [48,49]. The SEM cross-section images of

delaminated conductive silver paste layer resulting in charge separation due to the direct triboelectric effect occurring during damage are presented in Fig. S5.

Tests based on tensile and bending of the ZnO NWs-based composite were conducted by the same protocol. The changes in stress, piezoelectric voltage, and AE energy signal as a function of strain for ZnO-based composite laminate specimens during tensile and bending tests are plotted in Fig. 5e–f. During testing, both distribution and relative amplitude of AE energy emission followed similar trends as those obtained by composite laminates without ZnO NWs (Fig. 5c–d). Thus, the introduction of ZnO NWs may not alter the damage modes of composites. The coherence in both strain and relative amplitude between the sudden jumps of voltage generated by ZnO NWs and AE energy emissions during testing was not exactly 100%. However, a good correlation was still observed. For example, identical strain readings of 0.63% and 0.25% in voltage and AE emission measurements were noticed during tensile and bending tests, respectively. These corresponded to the first detectable damage, noted as the crack initiation strain. As strain increased, the sample became subjected to higher loads, causing more severe damage, as proved by higher amplitude of AE energy. The amplitude of AE energy emission has been correlated with damage severity in the prior studies [21,32,50,51]. The great coherence between the amplitude of voltage signals and AE energies validated the ability of ZnO NWs for classifying the damage severity using amplitude. In the early stage of testing, damage in the form of matrix cracking more likely occurred by evaluating the low amplitude of voltage and AE energy. However, high-level damage corresponding to interfacial debonding, interlaminar delamination, and fiber failure were expected to take place in the latter portion of the testing [32].

Additionally, to explore the all information about damage carried in the stress-strain curve, the strain-stiffness curves, representing the first derivative of the stress-strain curve, are plotted in Fig. S6a–b. Here, the stiffness is defined as the ratio of the axial stress difference and strain deference: $K = \Delta\sigma/\Delta\varepsilon$, where σ and ε refer to stress and strain, respectively. Note that the first derivative of the stress-strain curve could highlight the minuscule changes in the curves, which mark initiation and propagation of micro-fracturing in the composite [52]. One pulse on the strain-stiffness curve represented a high rise in stress caused by inner damage. The calculated sudden changes in strain-stiffness curves

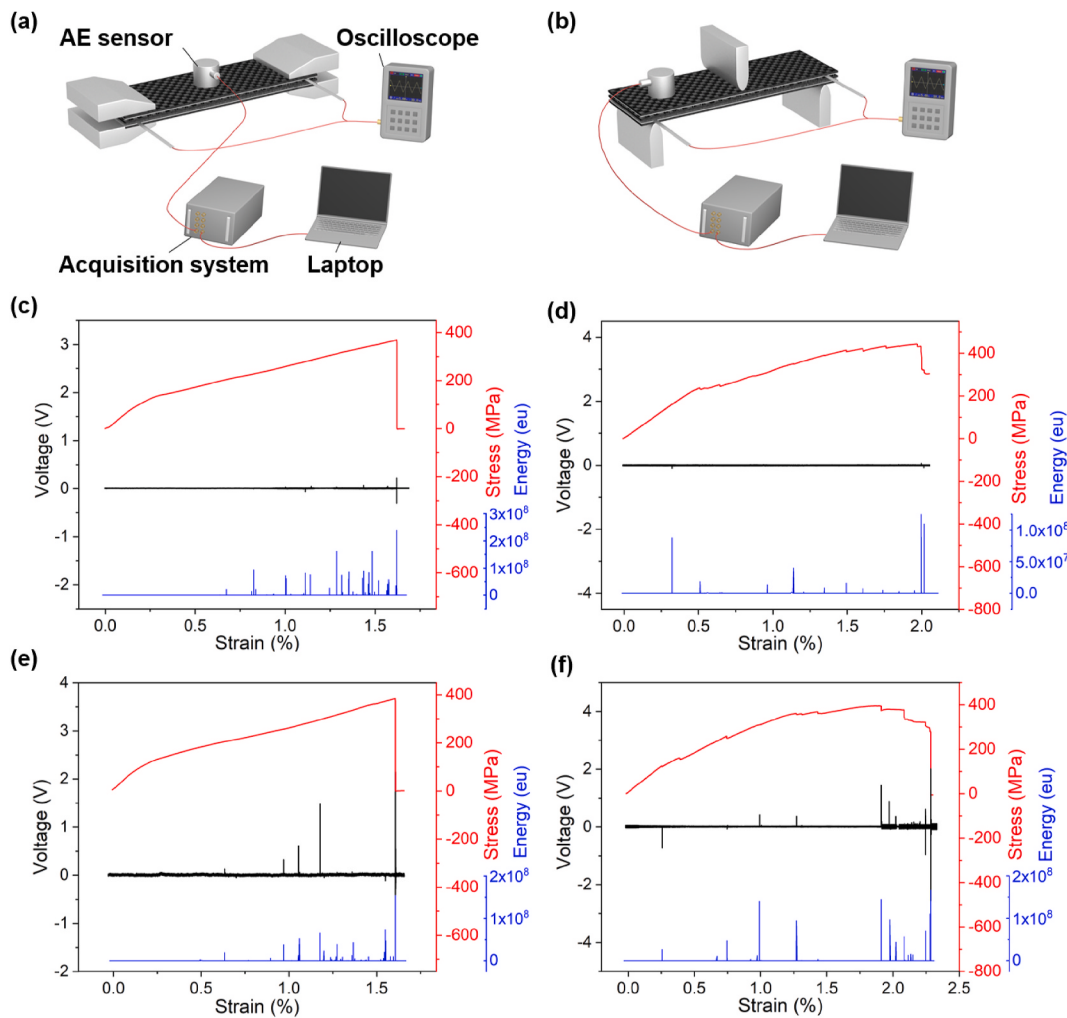


Fig. 5. Schematic representation of (a) tensile testing and (b) three-point bending testing setup with AE detection. The curves of stress, AE energy, and piezoelectric voltage responses versus strain for composite laminate without ZnO NWs obtained from tensile (c) and bending tests (d). The curves of stress, AE energy, and piezoelectric voltage responses versus strain for ZnO-based composite laminate obtained from tensile (e) and bending tests (f).

displayed excellent coherence with the strain of damage occurrence, amplitude of voltage, and AE energy. This further validated the ability of ZnO NWs for *in-situ* detection of composite damage in a comparable manner to the external bonded AE sensor.

Compared to ZnO-based composite, prevailing piezoelectric polymer P(VDF-TrFE)-based composites were prepared, and their abilities in *in-situ* damage self-monitoring were evaluated during tensile and three-point bending tests. The changes in stress, stiffness, and output voltage as a function of strain are gathered in Fig. S7. Compared to voltage signals obtained in ZnO-based composite, the strong piezoelectric characteristics made interleaved P(VDF-TrFE) thin film generate higher amplitudes of voltage readings during mechanical tests. Moreover, the dense voltage singles took place in early porting of testing, indicating the specimens experienced significant detectable damages. The first visible voltage peaks (crack initiation strain) in tensile and bending tests were estimated to be about 0.32% and 0.095%, respectively. These values were much smaller than those of ZnO-based composites. Therefore, the inclusion of P(VDF-TrFE) interleaf may introduce defects and cause damages during tests.

The incorporation of functional sensing materials, such as ZnO NWs and P(VDF-TrFE), in fiber-reinforced composites, would potentially increase the risk of damage due to the inclusion of foreign materials with different thermal and mechanical properties than the host composite. Hence, possible degradation in mechanical properties of the composites induced by interleaved sensing and implanted conductive electrodes

were evaluated by conducting the quasi-static tensile and three-point bending tests. To this end, a total of four samples (baseline composite, Ag-interleaved composite, ZnO-based, and P(VDF-TrFE)-based composites) were prepared by the manufacturing methodology shown in Section 2.3. Fig. 6 compares typical stress-strain curves and corresponding mechanical properties of the four specimens. As shown in tensile curves (Fig. 6a), Ag-interleaved composite and ZnO-based composite depicted nearly identical fracture strains and Young's moduli when compared to the baseline composite. Meanwhile, the introduction of ZnO NWs decorated carbon fabric into composite increased the tensile strength up to 392.47 ± 33.7 MPa (Fig. 6c), a value 7.4% larger than that of baseline composite (365.55 ± 14.1 MPa). This implies that dense rigid ZnO NWs might hinder the propagation of cracks and correspondingly enhance the composite's strength [43]. However, P(VDF-TrFE)-based composites illustrated a tensile strength of 260.89 ± 32.2 MPa (Fig. 6c), a value 28.6% smaller than that of the baseline composite laminate, suggesting P(VDF-TrFE) layer, epoxy, and fibers were not well bonded together. The flexural properties of the composites were investigated by three-point bending tests and the data are summarized in Fig. 6b–c. The stress-strain curves of all four composites displayed a similar linear portion, indicating almost equivalent flexural modulus of the composites. Compared to baseline composite laminate (462.86 ± 48.4 MPa), the inclusion of Ag conductive layer and P(VDF-TrFE) negatively impacted the flexural strength, which decreased by 8.8% and 82.4%, respectively. However, the introduction

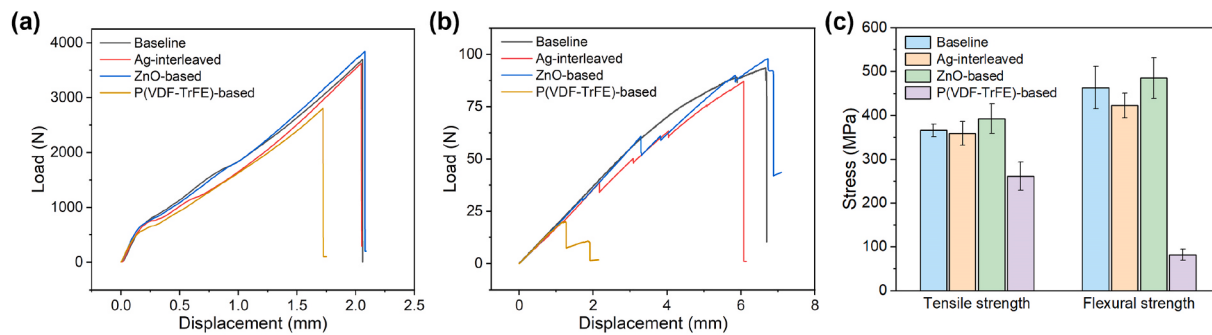


Fig. 6. Stress-strain curves of (a) tensile tests and (b) three-point bending tests. (c) Comparison of tensile and flexural strengths.

of ZnO NWs coated fabric into the composite slightly increased the flexural strength by 4.8%, reaching 485.26 ± 46.7 MPa. Therefore, the aforementioned results clearly demonstrated that the implantation of ZnO NWs in the composite did not only add self-sensing functionality but also provided inherent structural benefits to the host composite material.

To gain a better understanding of how interleaves (i.e., Ag conductive layer, ZnO decorated carbon fabric, and P(VDF-TrFE) layer) affect the tensile characteristics of laminates, the morphologies of fractured surfaces (baseline, Ag-interleaved, ZnO-based and P(VDF-TrFE)-based composites) were investigated. SEM side-sectional views of the four fractured composites specimens after tensile testing are gathered in Fig. 7. Cleanly delamination occurred between warp and weft tows at the interweave section in the plain-woven carbon fabric (Fig. 7a). Additionally, the introduction of Ag conductive layer increased the debonding damage possibility, as proved by the presence of cracks (white arrows in Fig. 7b–c). Therefore, Ag conductive layer might reduce the mechanical properties, consistent with data presented in Fig. 6c. Interfacial damage between fiber and epoxy could also be observed in Ag-interleaved and ZnO-based composite (Fig. 7b–c). The obvious differences were visible in changes in crack propagation path from the straight line in Ag-interleaved composite to a zigzag pattern in ZnO-based composite (white dash line). It means the crack propagation along interface in ZnO-based composite is longer and more fracture energy would be absorbed during the delamination, revealing that the well distributed ZnO NWs promote the formation of a mechanical interlock between carbon fiber and epoxy resin and consequently hinder and deflect the propagation of delamination crack. By contrast, the delamination cracks of P(VDF-TrFE)-based composite looked clean and

obvious (Fig. 7d). As shown in zoomed fractured surface, delamination cracks mainly propagated along the interface of P(VDF-TrFE) thin layer and epoxy, indicating weak interfacial bonding between fluorinated film and resin. This might be ascribed to the P(VDF-TrFE) thin film exhibiting low surface energy for bonding.

SEM images of fractured side-sections of the four composite specimens after three-point testing are depicted in Fig. 8. For baseline composite, Ag-interleaved composite, and ZnO-based composite samples, the increase in load led first to intra-laminar cracking within different carbon fabric layups. Subsequently, the cracks propagated longitudinally to the interlayer, which can be clearly observed in Fig. 8a–c. In addition, the two interfaces between conductive layers and epoxy underwent obvious delamination, meaning weaker bonding strength at these interfaces when compared to the others (Fig. 8b–c). Interestingly, the delamination cracking in P(VDF-TrFE)-based composite mainly propagated along the fluorinated film under extremely small loads, which can be certainly attributed to the weak interlayer properties. Compared to ZnO-based composite, the introduction of P(VDF-TrFE) thin layer into composite improved the sensitivity and voltage emission to microdamage. However, this did not provide structural benefit to the composite, and dramatically increased the risk of debonding and delamination. Correspondingly, the mechanical properties of composites deteriorated, as proved by Fig. 6c.

In practical applications, the functional composite would continuously withstand different levels of alternating stress. To gain a better understanding of the repetitive behavior of the composites, loading-unloading cyclic tensile tests comprising of 100 cycles at 3 mm/min speed were conducted to determine their stability. Here, the piezoelectric voltage output was continuously recorded for possible damage

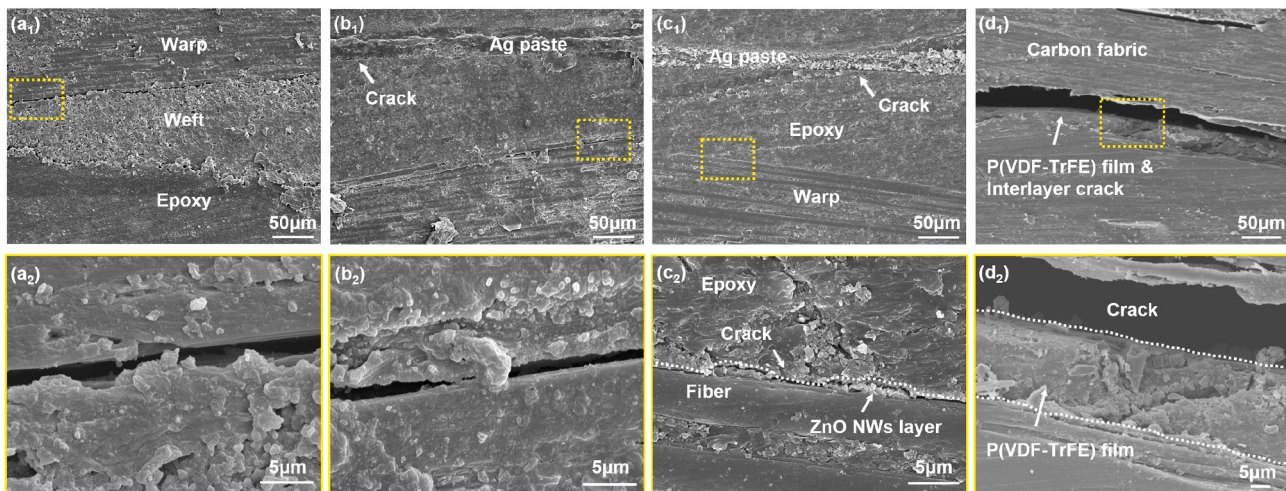


Fig. 7. SEM images of side-sectional morphology of fractured composites after tensile tests: (a) baseline composite, (b) Ag-interleaved composite, (c) ZnO-based composite, and (d) P(VDF-TrFE)-based composite.

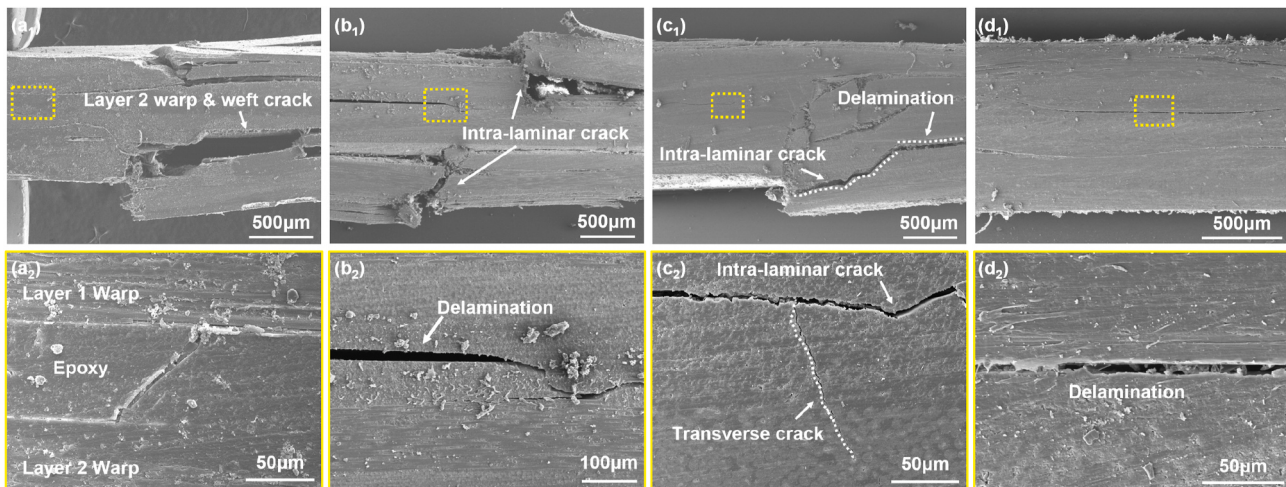


Fig. 8. SEM images of side-sectional morphologies of fractured composites after three-point bending tests: (a) baseline composite, (b) Ag-interleaved composite, (c) ZnO-based composite, and (d) P(VDF-TrFE)-based composite.

induced during the tests. The stress changes and voltage responses of ZnO-based composite at two tensile strains of 0.2% and 0.8% are provided in Fig. 9a–b, and corresponding stress-strain curves of the typical six cycles are shown in Fig. 9c–d. At applied strains of 0.2% and 0.8%, the functional composites showed a slight drop in stress at the beginning of cyclic loading, followed by nearly constant peak stress (Fig. 9a). This might be attributed to plastic deformation accumulated during the first few cycles of the loading-unloading process. In Fig. 9c–d, the stress increased linearly with the applied strain in the stage of small deformation of the first cycle, then followed by a nonlinear stress-strain plot. After relieving stress to zero, the strain did not return to its original value, indicating the occurrence of plastic deformation. Additionally, no obvious voltage response was detected during the cyclic tests under the applied strain of 0.2%, suggesting robustness of ZnO-based composite

lamines, suitable for operating normally under low-strain cycling conditions without obvious damage initiation. However, for the applied strain of 0.8%, which was much larger than the threshold strain value obtained in Fig. 5c, at which the tensile damage would initiate. As shown in Fig. 9b, several increasing steps of voltage were noticed, indicating that microdamage happened during cyclic tests at applied strain of 0.8%. However, peak stress remained constant, suggesting that voltage outputs were likely to be coherent with matrix cracking instead of severe damages.

4. Conclusions

In this work, piezoelectric ZnO NWs decorated carbon fabric was successfully prepared by a two-step growth method, which is interleaved

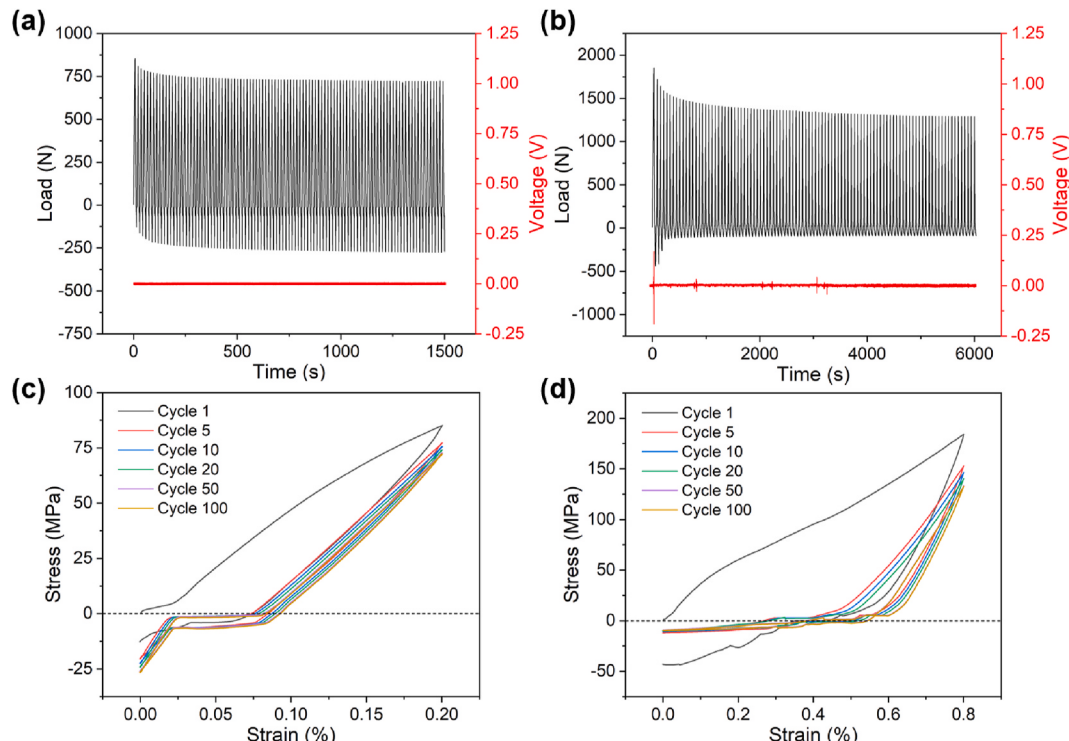


Fig. 9. Electromechanical characterization of ZnO-based composite. (a-b) The stress and piezoelectric voltage responses for 100 cycles under two different strains: (a) 0.2% and (b) 0.8%, (c-d) the six stress-strain cycles (No. 1, 5, 10, 20, 50, and 100) at strains of 0.2% and 0.8%.

into carbon fiber reinforced composite as a sensing component for *in-situ* damage monitoring. It is significantly different from the traditional embeddable sensors that additionally require power input and potentially increase the risk of degradation of the integrity of host composites. The proposed ZnO NWs-based sensing layer could generate a voltage emission resulting from composite damage without any external power source. Thus, the ZnO NWs interleaved composite has the ability to *in-situ* self-sensing damage, which is validated by the common AE damage detection method. Moreover, the ZnO NWs interleaf exhibited high compatibility and positive attributes with the host composites. The fully distributed nanowires grown on interleaved carbon fabric increased the interfacial bonded area and formed interlaminar mechanical interlocking morphology, and correspondingly improved the host composite's mechanical properties, which is superior to implanted strong piezoelectric PVDF flat film. Overall, the damage self-monitoring abilities with inherent structural advantages indicate that the ZnO NWs-based sensing approach is promising in the field of structural health monitoring.

Authorship statement

Xiaoming Chen: Conceptualization, Investigation, Funding acquisition, Writing. **Siyi Cheng:** Methodology, Validation, Investigation, Visualization, Writing - original draft. **Kaiqiang Wen:** Investigation, Analysis. **Chunjiang Wang:** Investigation, Analysis. **Jie Zhang:** Conceptualization, Supervision. **Han Zhang:** Methodology, Validation. **Hechuan Ma:** Data curation. **Lei Wu:** Methodology, Validation. **Tian-liang Li:** Validation, Conceptualization. **Baotong Li:** Methodology, Conceptualization. **Jinyou Shao:** Conceptualization, Resources.

All authors contributed to drafting of the manuscript. The manuscript is approved by all authors for publication.

Declaration of competing interest

The authors declare that they have no known competing financial interests or personal relationships that could have appeared to influence the work reported in this paper.

Data availability

Data will be made available on request.

Acknowledgements

The authors gratefully acknowledge support from the National Key Research and Development Program of China (No. 2020YFB1711300), the National Natural Science Foundation of China (NSFC) (Grant Numbers: 52175544, 52172098) and Fundamental Research Funds for the Central Universities (No. xzy022021011). The authors also thank the instrument Analysis Center of Xi'an Jiaotong University for the SEM and XPS work.

Appendix A. Supplementary data

Supplementary data to this article can be found online at <https://doi.org/10.1016/j.compositesb.2022.110368>.

References

- [1] Wen K, Ma H, Zhang J, Cheng S, Wang X, Hui Y, et al. Electrostatic excitation on fiber surface for enhancing mechanical properties of fiber-reinforced composite. Compos Sci Technol 2022;228:109627.
- [2] Aldave IJ, Bosom PV, González LV, De Santiago IL, Vollheim B, Krausz L, et al. Review of thermal imaging systems in composite defect detection. Infrared Phys Technol 2013;61:167–75.
- [3] D'Orazio T, Leo M, Guaragnella C, Distante A. Analysis of image sequences for defect detection in composite materials. In: International conference on advanced concepts for intelligent vision systems. Springer; 2007. p. 855–64.
- [4] Usamentiaga R, Venegas P, Guerendiaga J, Vega L, López I. Non-destructive inspection of drilled holes in reinforced honeycomb sandwich panels using active thermography. Infrared Phys Technol 2012;55(6):491–8.
- [5] Shepard DD, Smith KR. Ultrasonic cure monitoring of advanced composites. Sens Rev 1999;19:187–94.
- [6] Wang H, Dai J-G. Strain transfer analysis of fiber Bragg grating sensor assembled composite structures subjected to thermal loading. JCPBE 2019;162:303–13.
- [7] Fedorov A, Kosheleva N, Matveenko V, Srobaev. Strain measurement and stress analysis in the vicinity of a fiber Bragg grating sensor embedded in a composite material. GJCS 2020;239:111844.
- [8] Kim J-H, Park Y, Kim Y-Y, Shrestha P, Kim C-G. Aircraft health and usage monitoring system for in-flight strain measurement of a wing structure. Smart Mater Struct 2015;24(10):105003.
- [9] Wada D, Igawa H, Tamayama M, Kasai T, Arizono H, Murayama H, et al. Flight demonstration of aircraft fuselage and bulkhead monitoring using optical fiber distributed sensing system. Smart Mater Struct 2018;27(2):025014.
- [10] Wada D, Igawa H, Kasai T. Vibration monitoring of a helicopter blade model using the optical fiber distributed strain sensing technique. Appl Opt 2016;55(25):6953–9.
- [11] Wada D, Igawa H, Tamayama M, Kasai T, Arizono H, Murayama H. Flight demonstration of aircraft wing monitoring using optical fiber distributed sensing system. Smart Mater Struct 2019;28(5):055007.
- [12] Kwon H, Park Y, Kim J-H, Kim C-G. Embedded fiber Bragg grating sensor-based wing load monitoring system for composite aircraft. Struct Health Monit 2019;18(4):1337–51.
- [13] Aly K, Bradford PD. Real-time impact damage sensing and localization in composites through embedded aligned carbon nanotube sheets. Compos B Eng 2019;162:522–31.
- [14] Boztepe S, Liu H, Heider D, Thostenson ET. Novel carbon nanotube interlaminar film sensors for carbon fiber composites under uniaxial fatigue loading. Compos Struct 2018;189:340–8.
- [15] Groo L, Nasser J, Zhang L, Steinke K, Inman D, Sodano H. Laser induced graphene in fiberglass-reinforced composites for strain and damage sensing. Compos Sci Technol 2020;199:108367.
- [16] Groo L, Nasser J, Inman D, Sodano H. Laser induced graphene for in situ damage sensing in aramid fiber reinforced composites. Compos Sci Technol 2021;201:108541.
- [17] Yang G, Feng X, Wang W, OuYang Q, Liu L. Effective interlaminar reinforcing and delamination monitoring of carbon fibrous composites using a novel nano-carbon woven grid. Compos Sci Technol 2021;213.
- [18] Yang G, OuYang Q, Ye J, Liu L. Improved tensile and single-lap-shear mechanical-electrical response of epoxy composites reinforced with gridded nano-carbons. Compos Appl Sci Manuf 2022:152.
- [19] Reghat M, Mirabedini A, Tan AM, Weizman Y, Middendorf P, Bjekovic R, et al. Graphene as a piezo-resistive coating to enable strain monitoring in glass fiber composites. Compos Sci Technol 2021;211.
- [20] Li J, Zhang Z, Fu J, Liang Z, Ramakrishnan KR. Mechanical properties and structural health monitoring performance of carbon nanotube-modified FRP composites: a review. Nanotechnol Rev 2021;10(1):1438–68.
- [21] Yang G, Feng X, Wang W, OuYang Q, Liu L, Wu Z. Graphene and carbon nanotube-based high-sensitive film sensors for in-situ monitoring out-of-plane shear damage of epoxy composites. Compos B Eng 2021;204.
- [22] Gao L, Chou T-W, Thostenson ET, Zhang Z, Coulaud M. In situ sensing of impact damage in epoxy/glass fiber composites using percolating carbon nanotube networks. Carbon 2011;49(10):3382–5.
- [23] Lu S, Du K, Wang X, Tian C, Chen D, Ma K, et al. Real-time monitoring of low-velocity impact damage for composite structures with the omnidirectional carbon nanotubes' buckypaper sensors. Struct Health Monit 2019;18(2):454–65.
- [24] Xue L, Fan W, Yu Y, Dong K, Liu C, Sun Y, et al. A novel strategy to fabricate core-sheath structure piezoelectric yarns for wearable energy harvesters. Adv Fiber Mater 2021;3:239–50.
- [25] Choi M, Murillo G, Hwang S, Kim JW, Jung JH, Chen C-Y, et al. Mechanical and electrical characterization of PVDF-ZnO hybrid structure for application to nanogenerator. Nano Energy 2017;33:462–8.
- [26] Shin S-H, Kim Y-H, Lee MH, Jung J-Y, Seol JH, Nah J. Lithium-doped zinc oxide nanowires-polymer composite for high performance flexible piezoelectric nanogenerator. ACS Nano 2014;8(10):10844–50.
- [27] Zhang Y, Liu C, Liu J, Xiong J, Liu J, Zhang K, et al. Lattice strain induced remarkable enhancement in piezoelectric performance of ZnO-based flexible nanogenerators. ACS Appl Mater Interfaces 2016;8(2):1381–7.
- [28] Liao Q, Zhang Z, Zhang X, Mohr M, Zhang Y, Fecht H-J. Flexible piezoelectric nanogenerators based on a fiber/ZnO nanowires/paper hybrid structure for energy harvesting. Nano Res 2014;7(6):917–28.
- [29] Kim I, Roh H, Yu J, Jayababu N, Kim D. Boron nitride nanotube-based contact electrification-assisted piezoelectric nanogenerator as a kinematic sensor for detecting the flexion-extension motion of a robot finger. ACS Energy Lett 2020;5(5):1577–85.
- [30] Kim K-B, Jang W, Cho JY, Woo SB, Jeon DH, Ahn JH, et al. Transparent and flexible piezoelectric sensor for detecting human movement with a boron nitride nanosheet (BNNS). Nano Energy 2018;54:91–8.
- [31] Yuan L, Fan W, Yang X, Ge S, Xia C, Foong SY, et al. Piezoelectric PAN/BaTiO₃ nanofiber membranes sensor for structural health monitoring of real-time damage detection in composite. Compos Commun 2021;25:100680.
- [32] Groo L, Inman DJ, Sodano HA. In situ damage detection for fiber-reinforced composites using integrated zinc oxide nanowires. Adv Funct Mater 2018;28(35):1802846.

- [33] Haghiashtiani G, Greminger MA. Fabrication, polarization, and characterization of PVDF matrix composites for integrated structural load sensing. *Smart Mater Struct* 2015;24(4).
- [34] Hofmann P, Walch A, Dinkelmann A, Selvarayan SK, Gresser GT. Woven piezoelectric sensors as part of the textile reinforcement of fiber reinforced plastics. *Compos Appl Sci Manuf* 2019;116:79–86.
- [35] Groo L, Inman DJ, Sodano HA. Dehydrofluorinated PVDF for structural health monitoring in fiber reinforced composites. *Compos Sci Technol* 2021;214.
- [36] Coleman JN, Khan U, Blau WJ, Gun'ko. Small but strong: a review of the mechanical properties of carbon nanotube–polymer composites. *YKJC* 2006;44(9):1624–52.
- [37] Lee H, Dellatore SM, Miller WM, Messersmith. Mussel-inspired surface chemistry for multifunctional coatings. *PBJs* 2007;318(5849):426–30.
- [38] Postma A, Yan Y, Wang Y, Zelikin AN, Tjipto E, Caruso. Self-polymerization of dopamine as a versatile and robust technique to prepare polymer capsules. *FJCoM* 2009;21(14):3042–4.
- [39] Patterson BA, HAJAam Sodano. Enhanced interfacial strength and UV shielding of aramid fiber composites through ZnO nanoparticle sizing. *Interfaces* 2016;8(49):33963–71.
- [40] Lin YR, Ehlert G, Sodano HA. Increased interface strength in carbon fiber composites through a ZnO nanowire interphase. *Adv Funct Mater* 2009;19(16):2654–60.
- [41] Chen X, Wen K, Wang C, Cheng S, Wang S, Ma H, et al. Enhancing mechanical strength of carbon fiber-epoxy interface through electrowetting of fiber surface. *Compos B Eng* 2022;234:109751.
- [42] Wang B, Duan Y, Zhang J. A controllable interface performance through varying ZnO nanowires dimensions on the carbon fibers. *Appl Surf Sci* 2016;389:96–102.
- [43] Zheng N, Huang Y, Sun W, Du X, Liu H-Y, Moody S, et al. In-situ pull-off of ZnO nanowire from carbon fiber and improvement of interlaminar toughness of hierarchical ZnO nanowire/carbon fiber hybrid composite laminates. *Carbon* 2016;110:69–78.
- [44] Van Der Klift F, Koga Y, Todoroki A, Ueda M, Hirano Y, Matsuzaki R. 3D printing of continuous carbon fibre reinforced thermo-plastic (CFRTP) tensile test specimens. *Open J Compos Mater* 2016;6:18. 01.
- [45] Ye X, Cui Z, Fang H, Li X. A multiscale material testing system for *in situ* optical and electron microscopes and its application. *Sensors* 2017;17(8):1800.
- [46] Li L, Liu W, Yang F, Jiao W, Hao L, Wang R. Interfacial reinforcement of hybrid composite by electrophoretic deposition for vertically aligned carbon nanotubes on carbon fiber. *Compos Sci Technol* 2020;187.
- [47] Ye S, Cheng C, Chen X, Chen X, Shao J, Zhang J, et al. High-performance piezoelectric nanogenerator based on microstructured P(VDF-TrFE)/BNNTs composite for energy harvesting and radiation protection in space. *Nano Energy* 2019;60:701–14.
- [48] Chen C, Zhao S, Pan C, Zi Y, Wang F, Yang C, et al. A method for quantitatively separating the piezoelectric component from the as-received "Piezoelectric" signal. *Nat Commun* 2022;13(1):1391.
- [49] Šutka A, Sherrell PC, Shepelin NA, Lapčinskis L, Mālnieks K, Ellis AV. Measuring piezoelectric output—fact or friction? *Adv Mater* 2020;32(32):2002979.
- [50] Assrar M, Scida D, Zouari W, Saidane EH, Ayad R. Acoustic emission characterization of damage in short hemp-fiber-reinforced polypropylene composites. *Polym Compos* 2016;37(4):1101–12.
- [51] Chandarana N, Sanchez DM, Soutis C, Gresil M. Early damage detection in composites during fabrication and mechanical testing. *Materials* 2017;10(7):685.
- [52] Gao M-b, Li T-b, Meng L-b, Ma C-c, Xing H-l. Identifying crack initiation stress threshold in brittle rocks using axial strain stiffness characteristics. *J Mt Sci* 2018;15(6):1371–82.

Supporting materials

In Situ Damage Self-monitoring of Fiber-reinforced Composite by Integrating Self-powered ZnO Nanowires Decorated Carbon Fabric

Xiaoming Chen,¹ Siyi Cheng,¹ Kaiqiang Wen,¹ Chunjiang Wang,¹ Jie Zhang,^{2,*} Han Zhang,¹ Hechuan Ma,¹ Lei Wu,³ Tianliang Li,⁴ Baotong Li,^{5,*} Jinyou Shao¹

¹Micro- and Nanotechnology Research Center, State Key Laboratory for Manufacturing Systems Engineering, Xi'an Jiaotong University, Xi'an, Shaanxi, 710049, China

²Electronic Materials Research Laboratory, Key Laboratory of the Ministry of Education & International Center for Dielectric Research, School of Electronic Science and Engineering, Xi'an Jiaotong University, Xi'an, Shaanxi, 710049, China

³School of Petroleum Engineering, China University of Petroleum (East China), Qingdao, 266580, China

⁴School of Mechanical and Electronic Engineering, Wuhan University of Technology, Wuhan, China

⁵Key Laboratory of Education Ministry for Modern Design & Rotor-Bearing System, Xi'an Jiaotong University, Xi'an, Shaanxi, 710049, China

*To whom correspondence should be addressed. jzhang12@xjtu.edu.cn (J. Zhang) and baotong.me@xjtu.edu.cn (B. Li)

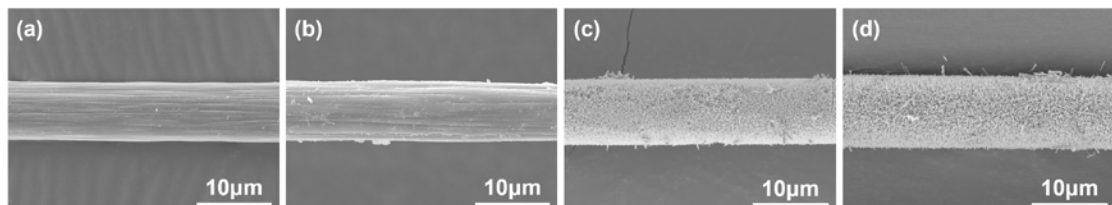


Figure S1: SEM image of (a) pristine T300 carbon fiber; (b) carbon fiber covered by ZnO seed layer; (c-d) carbon fiber covered with ZnO NWs (growth time of 2h and 6h)

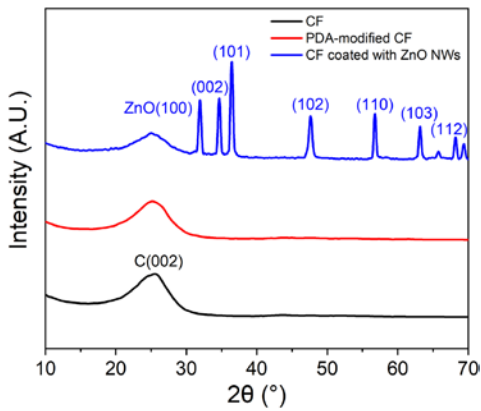


Figure S2: XRD spectra of CF, PDA-modified CF and ZnO NWs-coated CF.

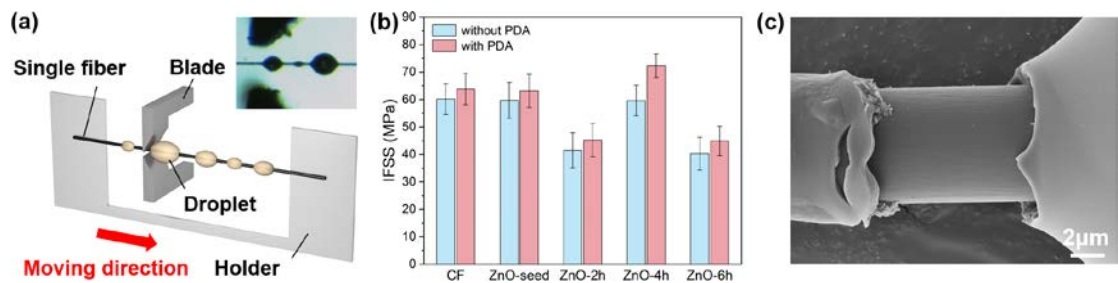


Figure S3: (a) Schematic diagram of measuring IFSS by the microdroplet debonding test and representing microdroplet for debonding test. (b) Effect of PDA treatment and ZnO NWs with different growing times on interfacial shear strength of carbon fiber-EP interface. (c) SEM image of debonded surface of ZnO NWs coated CF-EP interface (growth time of ZnO NWs is 2 h).

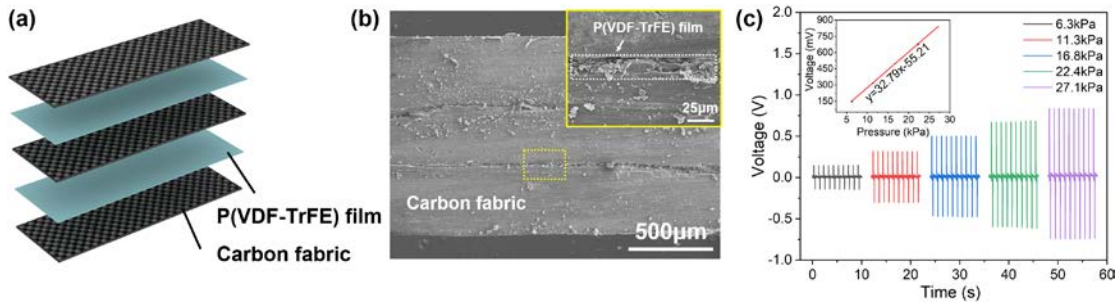


Figure S4: (a) Explosion diagram of P(VDF-TrFE)-based composite laminate. (b) SEM cross-sectional image of P(VDF-TrFE)-based composite laminate, the inset represents the interleaved piezoelectric film P(VDF-TrFE). (c) Dependence of output voltages on different applied forces.

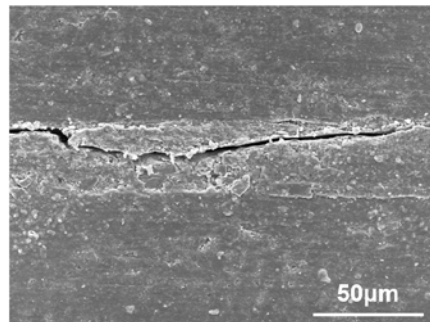


Figure S5: SEM cross-sectional image of fractured composite laminate after tensile test.

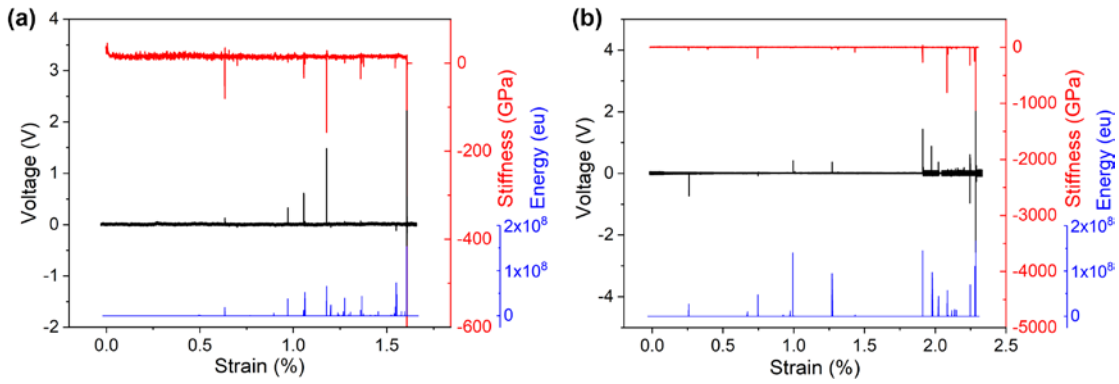


Figure S6: The curves of stiffness, AE energy and piezoelectric voltage responses versus strains for ZnO-based composite laminate obtained from (a) tensile and (b) bending tests.

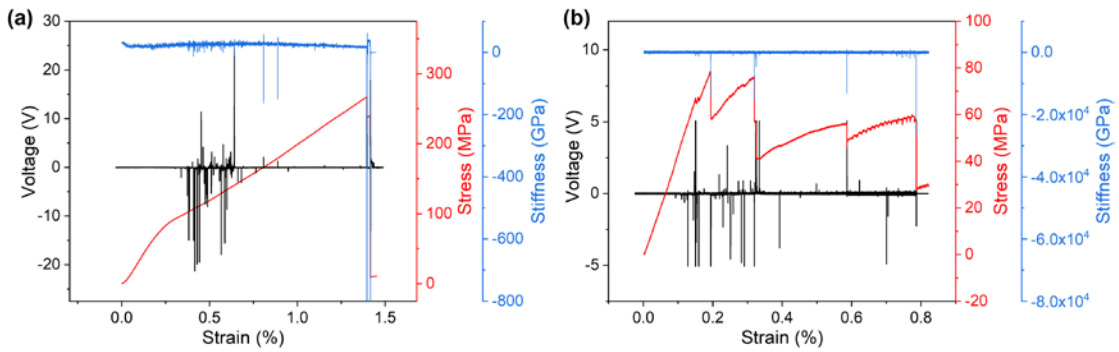


Figure S7: The curves of stress, piezoelectric voltage responses and stiffness versus strain for P(VDF-TrFE)-based composite obtained from (a) tensile test and (b) three-point bending test.